Journal of Fusion Energy, Vol. 14, No. 1, 1995

A Two-Fluid Code for the Thermohydraulic Transient Analysis of CICC Superconducting Magnets

R. Zanino,[1] S. De Palo,[1] and L. Bottura[2]

We present here a finite element computer model (Mithrandir) for the transient thermohydraulics of compressible helium in a Cable-In-Conduit Conductor (CICC) with central cooling hole, as presently envisaged for superconducting magnets of the International Thermonuclear Experimental Reactor (ITER). In the model the He in the hole and that in the cable bundle are treated as separate fluids, each characterized by its own flow and thermodynamic properties, coupled by exchanges of mass, momentum and energy. Results for the simulation of a quench both with and without a wall delimiting the central cooling hole are discussed. Time and space convergence of the code are demonstrated numerically.

KEY WORDS: Superconducting magnets; cable-in-conduit-conductors; quench; helium thermohydraulics; numerical methods.

1. INTRODUCTION

Most of the existing computer codes for the analysis of a quench transient in a superconducting magnet treat the He coolant as a single fluid. This is obviously justified whenever the geometry of the cooling channel is such that one can reasonably expect little inhomogeneities in any cross section. On the other hand, the present design of CICC for the ITER magnets includes a central cooling hole to the purpose of increasing the flow at given pressure head. Clearly, assuming in this situation quasihomogeneous properties for all the He, both in the cable bundle surrounding the hole and in the hole, will become less and less correct, the more the radial mixing between the two regions is impeded.

Recently[1] a first step towards a more general treatment of this situation was taken, including in the code Gandalf the possibility of different He flow velocities in the cable bundle and in the hole, though still retaining same thermodynamic state for both (i.e., same pressure *and* temperature) at any given section. If He crossflow is not fully impeded, which would probably be unreasonable from an engineering point of view, the question of how good the assumption of same thermodynamic state is, reflects to the question of which timescale one wants to model. Pressure equalization will happen on a very fast (sound) time scale, much faster that the typical (order of 1 second) timescale of the quench; however, temperature equalization will require a significantly longer time (order of the reciprocal of the transverse Mach number of the flow); therefore, we felt the need to develop a model which would be both more complete from the physics point of view, and efficient on all time scales of interest.

Here we present a 1-D, two-fluid model, Mithrandir, where the He in the cable bundle and that in the hole can have different velocities *and* different thermodynamic state. The fluids are coupled between themselves by mass, momentum and energy exchange, and with the conductor strands and jacket by convective energy transport. The model is described in Sec. 2, including choice of dependent thermodynamic variables, equations and boundary conditions; the numerical

[1] Dipartimento di Energetica, Politecnico, I-10129 Torino, Italy.
[2] CERN, Division AT-MA, CH-1211 Geneva 23, Switzerland.

0164-0313/95/0300-0025$07.50/0

method for space and time discretization of the model is discussed in Sec. 3; to assess the validity of the code a rather detailed set of computational tests and convergence studies has been performed, and its results are summarized in Sec. 4. The code has in parallel been validated against experimental data, as reported in.[2] A model similar to that implemented in Mithrandir, although based on different state variables, is also being used elsewhere.[3]

2. DESCRIPTION OF THE MODEL

We consider the transient flow of low temperature supercritical He in a CICC, under the action of heating sources in the strands and in the jacket.

Observing that the typical transversal size of the conductor is several orders of magnitude smaller than its length, it is customary to straighten it out (which is justified by the relatively large, O(1m) curvature radii) and assume a *one-dimensional* treatment in the x-coordinate along its length to be sufficient. The equations are therefore derived from the 3-D case by appropriate averaging over (portions of) the cross section.

The second important approximation made in the model is to assume essentially *ideal* flow conditions, with dissipation concentrated in a Fanning factor viscosity, but without any second order derivatives in x: from the (restrictive) point of view of a single fluid the model therefore resembles that of the Euler system of equations, and this has important implications on the numerical treatment (see below).

The model presented here heavily relies, *nomen omen*, on that of[1] but extends it in two major respects: (1) three equations for each fluid (He in the cable bundle and He in the hole) are solved simultaneously, for a total of 6 fluid equations (then further coupled to heat conduction in the strands and in the jacket), as opposite to[1] where 4 fluid equations were solved (only the flow velocities were allowed to be different); (2) mass, momentum and energy exchanges between the two fluids need be modeled by appropriate coupling terms. The interested reader will find in[1] details of the model not directly referring to the points just mentioned.

2.1. Choice of Thermodynamic State Variables for the He

The choice of thermodynamic variables for the description of the He state is by no means unique or straightforward, and different answers to this question can be found in the literature. We believe that this choice can be influenced by three principal facts, among others: (1) conservative vs. nonconservative form; (2) behavior of the coefficients in the fluid equations near the critical point and across the transposed critical line; (3) need for implicit treatment of certain driving terms related to the stiffness of the system of equations. We are now going to briefly address each of these points in the following.

As to the first point it is well known that the advantages of a conservative form appear most clearly in the presence of flow discontinuities, e.g., shocks. To rigorously exclude this occurrence will need a more careful investigation in the future; however, for the present, very low Mach numbers M are expected in our problem (*a posteriori* we found max(M) = a few % in some of the cases presented here), i.e., we should be fairly far from the possible insurgence of steady discontinuities in the flow; furthermore, viscosity, and heat conduction in the cables, should provide some broadening mechanism for possible unsteady discontinuities, at least for the bundle He. On the other hand, using the mass density ρ and the total energy density e as variables could force us to treat explicitely/iteratively strong driving terms, e.g., the pressure gradients in the momentum equations, or else go through delicate interpolations in the tables of thermodynamic properties. Since we consider implicit time marching as a must for this problem (see below) we will therefore use equations in non conservative form.

As to the second point one can observe that there are two major possibilities as nonconservative state variable couples, namely: (a) pressure p and specific enthalpy w, or (b) p and temperature T. In Ref. 4, it is shown that for steady single fluid flow the coefficients in the equation for dT/dx suffer strong variations near the critical point and across the displaced critical line, therefore this feature could in principle lead to difficulties also in the numerical solution of our problem if choice b was taken.

As to the third point, on the other hand, if one uses choice a (or, for that matter, conservative variables) the strong coupling terms due to heat convection between the strands and the helium, which are proportional to T, would need to be treated explicitely/iteratively. The time scale of this term can be much faster than the time scale of the quench, i.e., the problem is *stiff*; this explicit treatment must then be avoided, because it would need extremely low time steps Δt, and therefore make the simulation of the whole transient very expensive; furthermore, the coefficients in our model seem not to undergo dramatic changes, because we are and typically stay fairly far from the critical point. For the above reasons we will use p and T as state variables for the helium; to establish the actual importance in the case at hand of the discussion in[4] particularly on the issues of linearization (see below) and stability, will need a more thorough study which is beyond the scope of this paper.

2.2. Equations and Boundary Conditions

The equations in our model describe the nonlinear time evolution of the vector of unknowns

$$\mathbf{u} = [v^B,\ p^B,\ T^B,\ v^H,\ p^H,\ T^H,\ T_{St},\ T_{Jk}]^t$$

under the action of external and/or Joule heat sources.

2.2.1. Helium Fluids

The set of equations in v, p and T variables has been derived for *each* of the two fluids from the general conservative form of mass balance (with a mass source Λ_ρ), momentum balance along x (with a momentum source Λ_v) and total energy balance (with an energy source Λ_e). With straightforward algebra we obtain

$$\frac{\partial v}{\partial t} + v\frac{\partial v}{\partial x} + \frac{1}{\rho}\frac{\partial p}{\partial x} = \frac{1}{\rho}[\Lambda_v - v\,\Lambda_\rho] \qquad (1)$$

$$\frac{\partial p}{\partial t} + \rho c^2\frac{\partial v}{\partial x} + v\frac{\partial p}{\partial x} = \phi\,[\Lambda_e - v\Lambda_v - (w - \frac{v^2}{2} - \frac{c^2}{\phi})\,\Lambda_\rho] \qquad (2)$$

$$\frac{\partial T}{\partial t} + \phi T\frac{\partial v}{\partial x} + v\frac{\partial T}{\partial x} = \frac{1}{\rho c_v}[\Lambda_e - v\Lambda_v - (w - \frac{v^2}{2} - \phi c_v T)\,\Lambda_\rho] \qquad (3)$$

where, in particular, Eq. (2) is derived "from" the mass balance. Here v is the fluid velocity along x, c is the sound speed, $\phi \equiv (\rho/T)(\partial T/\partial\rho)_s$ is the Gruneisen parameter (see Ref. 4), and c_v is the specific heat at constant volume. Once p and T are known, then ρ, θ, and the parameters c, ϕ, c_v can be obtained from tables.[5] (Each equation (1–3) is used twice: once for the He in the cable bundle, once for the He in the hole, with the respective values of the parameters).

Notice that in Eq. (1) no gravity force is present because it is negligible for the limited elevation differences in the magnets. Also, viscosity effects are concentrated in a friction factor, see Eq. (3a), as customary in one-dimensional internal flow, and heat conduction is assumed in Eqs. (2–3) to be negligible due to the extremely low heat conductivity of He (see Sec. 4.1).

Table I. Data Used for the Simulations

Parameter	Value	
Conductor length	10	[m]
Helium cross section in hole	19.63	[mm2]
Helium cross section in bundle	88.85	[mm2]
Nb_3Sn cross section	47.5	[mm2]
Copper cross section	66.5	[mm2]
Steel cross section	66.67	[mm2]
Insulation cross section	0.0	[mm2]
Conductor Strain	−0.0025	
Copper RRR	100	
Conductor-Helium bundle wetted perimeter	371.1	[mm]
Jacket-Helium bundle wetted perimeter	54.0	[mm]
Conductur-Jacket wetted perimeter	1.0	[mm]
Hydraulic diameter of hole	5.0	[mm]
Hydraulic diameter of bundle	0.86	[mm]
Operating current (constant)	8.0	[kA]
Magnetic field (constant)	11.0	[T]
Energy deposited into strands	10.0	[kJ/m]
Heater length	0.2	[m]
Pulse duration	1.0	[s]
Helium inlet temperature	5.0	[K]
Helium inlet pressure	0.6	[MPa]
Helium outlet pressure	0.6	[MPa]

As to the sources, Λ_ρ comes wholly from the mixing between the two fluids and is discussed, together with the other terms with the same origin, in the next section. For the momentum source we have

$$\Lambda_v = \Lambda_v^{\text{mix}} - F\cdot\rho \quad with \quad F \equiv 2f\,\frac{v|v|}{D} \qquad (3a)$$

where f is the Reynolds number dependent friction factor and D is the hydraulic diameter. For the heat source we have to explicitely distinguish between He in the cable bundle (index B), which directly exchanges energy by convection with strands and jacket Λ_e^{JS}, and He in the hole (index H), which in our model exchanges energy only with the He in the bundle; correspondingly we have

$$\Lambda_e^B = \Lambda_e^{JS} - P_{\text{eq}}\,h_{\text{eq}}\,(T^B - T^H)/A_B + \Lambda_e^{\text{mix},B}$$

with

$$\Lambda_e^{JS} \equiv [P_{St}\,h_{St}\,(T_{St} - T^B) + P_{Jk}\,h_{Jk}\,(T_{Jk} - T^B)]/A_B \qquad [3b]$$

whereas

$$\Lambda_e^H = P_{\text{eq}}h_{\text{eq}}\,(T^B - T^H)/A_H + \Lambda_e^{\text{mix},H} \qquad (3c)$$

Here P are the wetted perimeters, h the corresponding convective heat transfer coefficients (see Ref. 1 for de-

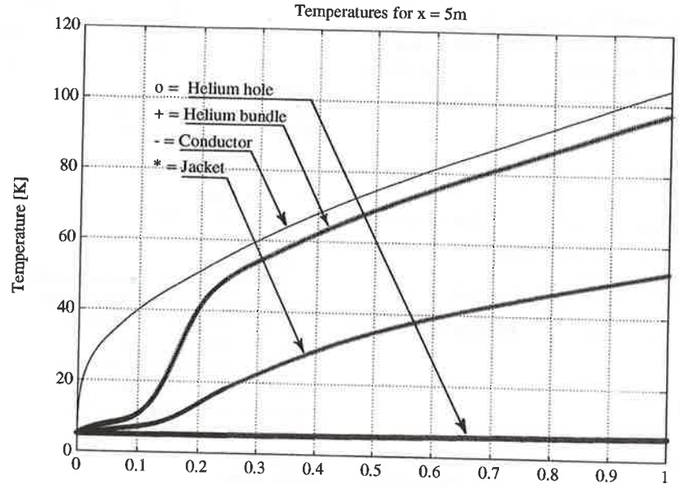

Fig. 1a. Temperatures [K] at $x = 5$ m vs. time [s]: strands (solid line), cable bundle He (+), jacket/conduit (*), hole He (○).

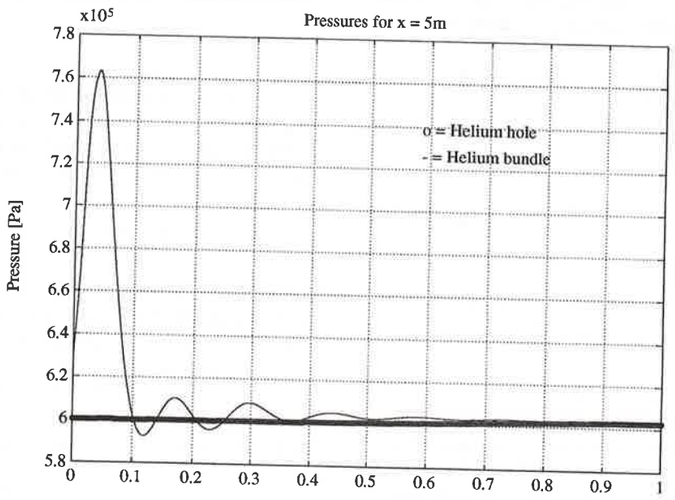

Fig. 1b. He pressures [Pa] vs. time [s]: cable bundle (solid line), hole (○).

tails), A_B is the cross-sectional area of the He channel in the cable bundle. Indices *St* and *Jk* refer to the strands and to the conduit/jacket respectively.

Boundary conditions for each triplet of equations can be imposed subject to the restrictions from characteristics theory: assuming subsonic flow everywhere in the channel, at an inlet section two characteristics (v and $v + c$) will be ingoing, therefore two boundary conditions must be imposed; at an outlet section only one characteristic ($v - c$) will be ingoing, therefore one boundary condition is needed. We typically use: given p and T at an inlet, given p at an outlet. More general boundary conditions, e.g., including flow, could be considered.

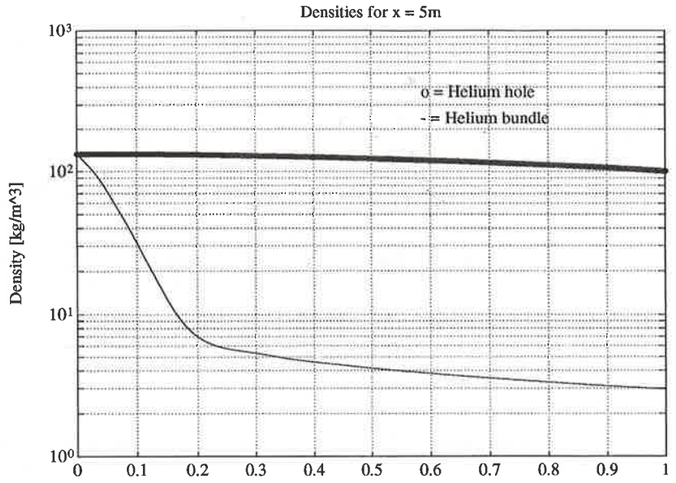

Fig. 1c. He densities [kg/m³] vs. time [s]: cable bundle (solid line), hole (○).

2.2.2. Modeling of Mixing Terms

We express each of the mass sources in Eqs. (1–3) as follows

$$\Lambda_\rho = \frac{\Gamma_\rho}{\ell A} \tag{4a}$$

where ℓ is the pipe length,

$$\Gamma_\rho^H = \tilde{\rho} v_\perp A_\perp \quad \Gamma_\rho^B = -\Gamma_\rho^H \tag{4b}$$

Here the perpendicular flow velocity is deduced by treating the bundle/hole interface as a concentrated loss in a hydraulic circuit, with loss coefficient κ

$$v_\perp = \sqrt{\frac{2|p^H - p^B|}{\kappa \tilde{\rho}}} \frac{p^B - p^H}{|p^B - p^H|} \tag{4c}$$

The ''tilde'' variables, here as in the following, refer to bundle values if $v_\perp > 0$, to hole values viceversa. The perpendicular cross section $A_\perp$ is to be given by the user, but will actually have to come together with κ from a detailed model of the interface (see, e.g., Ref. 6).

The momentum exchange between He in the hole and He in the bundle is given by

$$\Lambda_v^{\text{mix}} = \frac{\Gamma_v}{\ell A} \tag{5a}$$

$$\Gamma_v^H = \lambda_v \Gamma_\rho^H \tilde{v} \quad \Gamma_v^B = -\Gamma_v^H \tag{5b}$$

i.e., we assumed a purely convective exchange of momentum. The parameter λ_v attempts to qualitatively take into account the structure of the material interface: if this is such that it absorbs most of the momentum, as in the case of a wall with small holes, then $\lambda_v \approx 0$; in the opposite case of, say, a spiral with long pitch, $\lambda_v \approx 1$.

For the heat/enthalpy exchange between the two flows we have

$$\Lambda_e^{\text{mix},H} = \frac{\Gamma_\rho^H [\tilde{w} + (\lambda_v \tilde{v})^2/2]}{\ell A_H} + \frac{P_{HB} h_{HB} (T_B - T_H)}{A_H} \tag{6a}$$

$$\Lambda_e^{\text{mix},B} = \frac{\Gamma_\rho^B [\tilde{w} + (\lambda_v \tilde{v})^2/2]}{\ell A_B} + \frac{P_{HB} h_{HB} (T_H - T_B)}{A_B} \tag{6b}$$

i.e., we consider a more general situation, including both convective (depending on Γ_ρ) and conductive (depending on the interface wetted perimeter P_{HB} and heat transfer coefficient h_{HB}, see Ref. 6) contributions.

2.2.3. Conduit and Strands

Both conduit and strands can be approximately modeled with the same kind of one-dimensional heat conduction equation

$$A_i \rho_i C_i \frac{\partial T_i}{\partial t} - A_i \frac{\partial}{\partial x}\left(K_i \frac{\partial T_i}{\partial x}\right) = - Q_{\text{He},i} + Q_{\text{Joule},i} + Q_{\text{ext},i} - Q_{ik} \qquad i = St, Jk \tag{7}$$

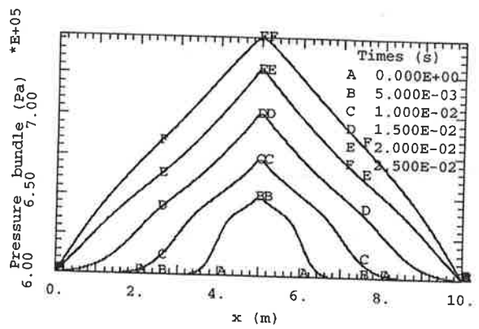

Fig. 2a. Time evolution of the cable bundle He pressure profiles, over the first 0.025s.

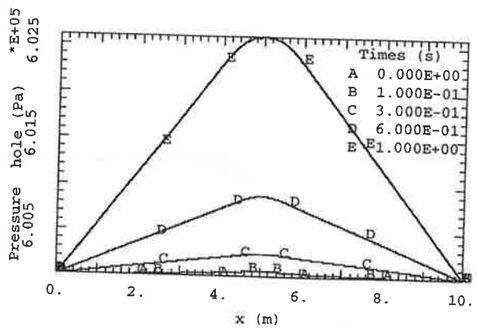

Fig. 2b. Time evolution of the hole He pressure profiles, over the first 1s.

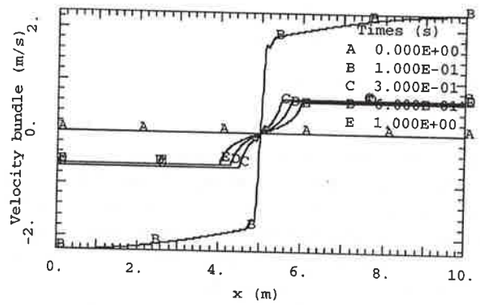

Fig. 2c. Time evolution of the cable bundle He flow velocity [m/s] profiles, over the first 1s.

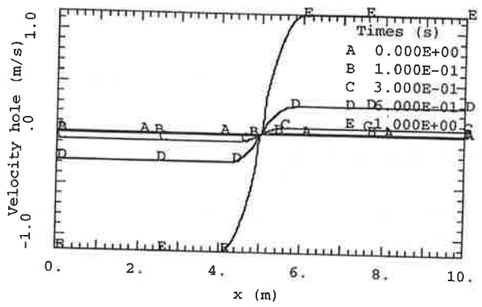

Fig. 2d. Time evolution of the hole He flow velocity profiles, over the first 1s.

where A is the total cross sectional area, C the mass averaged specific heat, K the area averaged heat conductivity. As to the sources at the righthand side: $Q_{He,St} + Q_{He,Jk} = \Lambda_e^{JS} A_B$; Joule and external (e.g., friction, nuclear, etc.) heat sources have been included; finally, Q_{ik} represents the direct (contact) internal heat exchange between strands and conduit.

Typically, adiabatic conditions at the pipe ends are assumed for both conduit and strands.

3. NUMERICAL METHOD

A finite element Galerkin method with linear (P_1) test and trial functions is used for space discretization of Eqs. (1–3,7), augmented by stabilizing numerical diffusion terms. The space integrals in the elemental matrix are computed numerically using the one point Gauss (midpoint) rule. The mesh is adapted in time according to the needs of resolution of strong gradients which appear at the (moving) normal front during the transient.

The resulting set of nonlinear ODEs is discretized in time with finite differences, with a general approach including the whole range between explicit and fully implicit method; from this we get a nonlinear system of algebraic equations which is first linearized and then solved at each time step by a standard direct algorithm for banded matrices. Also the time step can be varied in time, according to the particular time scale which is being followed at that instant of the transient (see below and Ref. 1 for details).

3.1. Space Discretization on an Adaptive Mesh

The Galerkin method (see, e.g., Ref. 7) is standard and we will not discuss it here. For elliptic problems it

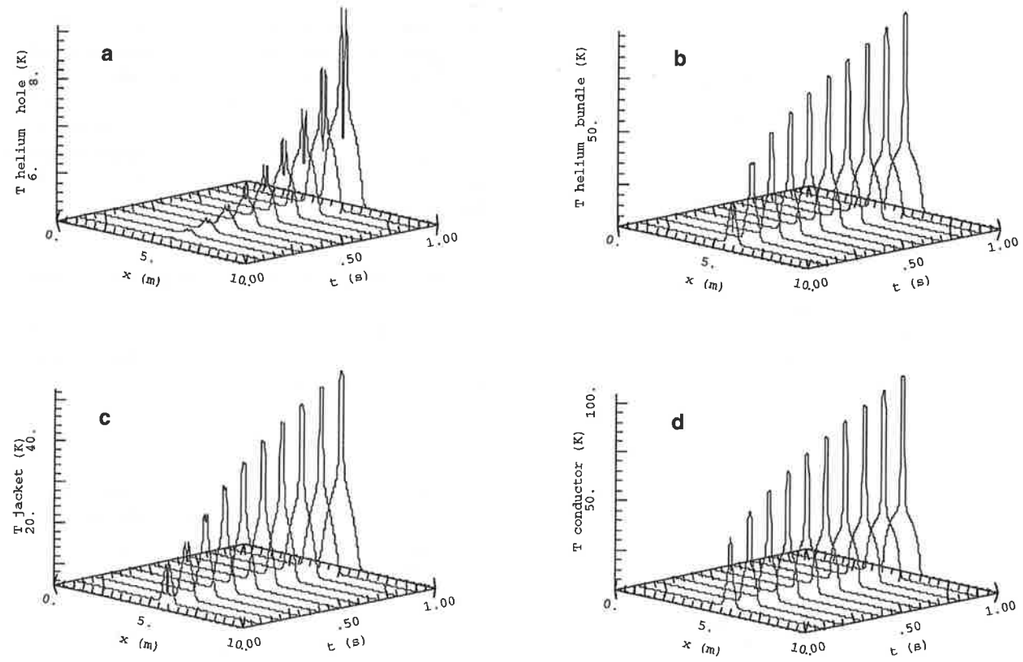

Fig. 3. Space/time temperature profiles: hole He (a), cable bundle He (b), jacket/conduit (c), strands (d).

provides an optimal discretization, but if the problem tends to become hyperbolic (e.g., where convection dominates over conduction/diffusion) then spatial unphysical oscillations arise whenever one is not resolving with a sufficiently fine mesh internal/boundary layers. Since this behavior is obviously undesired one can try to treat this situation by at least two different means: (1) locally refine the mesh wherever strong gradients appear; (2) include some kind of numerical dissipation to make the problem less convection dominated (see Sec. 3.2).

For the application at hand the advantages of an adaptive mesh have been first recognized in,[8] and details of the method used in Mithrandir can be found in.[1] Instead of searching for large gradients in the solution we use as "error" indicator the localization of the normal front, near which significant spatial variations are expected to take place. Starting from an initial background mesh which is never changed we add and/or subtract nodes, refining the mesh according to a Gaussian density distribution centred at the front, and removing them as soon as the front has moved sufficiently further away. A maximum (typically the initial, fixed one) and a minimum size of the elements can be prescribed by the user.

3.2. Stabilization by Means of Local Artificial Diffusion

As a further, parallel means of avoiding oscillations in the solution we have added to the ith right-hand side in Eqs. (1–3) a numerical diffusion term

$$\frac{\partial}{\partial x}\left[g_i \frac{\partial u_i}{\partial x}\right] \qquad i = 1,\ldots,6 \tag{8a}$$

with *local* diffusion coefficient

$$g_i = \alpha_i \frac{|v|\Delta x}{2} \tag{8b}$$

The choice $\alpha_i = 1$ amounts to using the prescription of the Streamline-Upwind Petrov-Galerkin (SUPG) scheme,[7] although weighting with the correspondingly modified test function the convective terms only. Pure

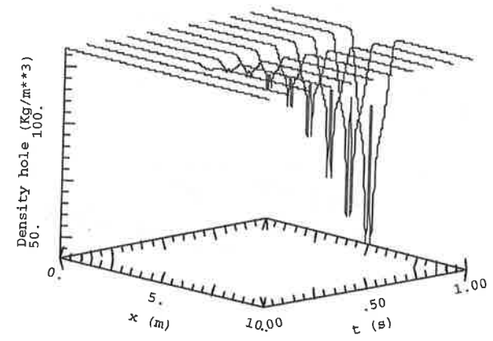

Fig. 4. Space/time He density profiles: hole (a), cable bundle (b).

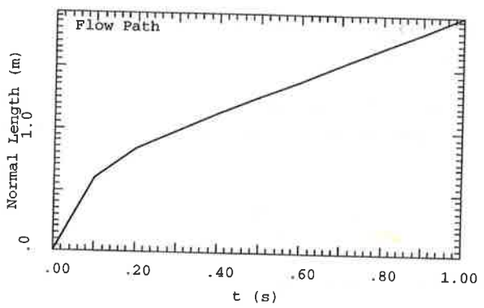

Fig. 5. Length of normal conducting region [m] vs. time.

Galerkin weighting of the time dependent and source terms, as we do here, has been shown to lead in some cases to significant errors;[7] however, also these errors obviously vanish with Δx (see Eq. 8b), and will become less important if a sufficiently fine mesh is used where large gradients in the sources and or large variations in time appear. Here we shall check numerically in some cases that the solutions obtained with $\alpha_t = 1$ are not too far from those obtained with the pure Galerkin method (i.e., with $\alpha_t = 0$); the need for, and implementation of a full SUPG for the problem at hand will be considered elsewhere.

3.3. Time Discretization with Adaptive Time Step

Once the set of Eqs. (1–3,7) has been discretized in space over a mesh with, say, N nodes, we are left with a set of nonlinear ODEs

$$M \frac{dU}{dt} = L(U) = A(U)\,U \qquad U = [\mathbf{u}'_{x1}, \mathbf{u}'_{x2}, \ldots, \mathbf{u}'_{xN}]' \quad (9)$$

where M is the so called mass matrix (see Refs. 1 and 7) and U is the discretized vector of unknowns.

The θ-method is then used to advance U forward in time from t (index n) to $t + \Delta t$ (index $n + 1$) and Eq. (9) becomes

$$M \frac{U^{n+1} - U^n}{\Delta t} = (1 - \theta) L(U^n) + \theta L(U^{n+1}) \qquad 0 \le \theta \le 1 \quad (10)$$

If M was lumped (diagonalized) then $\vartheta = 0,\ 0.5,\ 1$ would lead to the explicit, Crank-Nicolson and fully implicit schemes, respectively.

The time step Δt can be varied during the transient. This is a simple matter for a two-level time stepping algorithm, and is one of the reasons for the choice of the ϑ-implicit method. Essentially, two thresholds ε_1 and $\varepsilon_2 > \varepsilon_1$ for the absolute value of the maximum (over all unknowns and over the whole pipe) relative variation ε of a U component are defined by the user. If $\varepsilon < \varepsilon_1$ then Δt is increased by a factor $\mu_1 > 1$; if $\varepsilon_1 \le \varepsilon \le \varepsilon_2$ then Δt is unchanged; finally, if $\varepsilon > \varepsilon_2$ then Δt is reduced by a factor $\mu_2 > 1$ (both μ_1 and μ_2 are chosen by the user). No step is thus ever rejected. This "explicit" prediction of the time step based on the result of the previous step obviously is a good choice for small steps only; however, accuracy constraints would force us to use not too large steps anyway, in order to follow the advancing normal front.

3.4. Linearization

Unless $\theta = 0$, Eq. (10) is a set of nonlinear equations because of the nonlinearity in the evolution operator L. Several possible ways would be available to linearize Eq. (10), e.g., from the family of Newton or quasi-Newton methods. For the sake of simplicity we choose here to freeze A at the previous time step and linearize Eq. (10) according to

$$L(U^{n+1}) = A(U^{n+1})U^{n+1} \approx A(U^n)U^{n+1} \qquad (10a)$$

A detailed study of the effects of this choice and of the tradeoffs against other possible linearizations is currently under way.

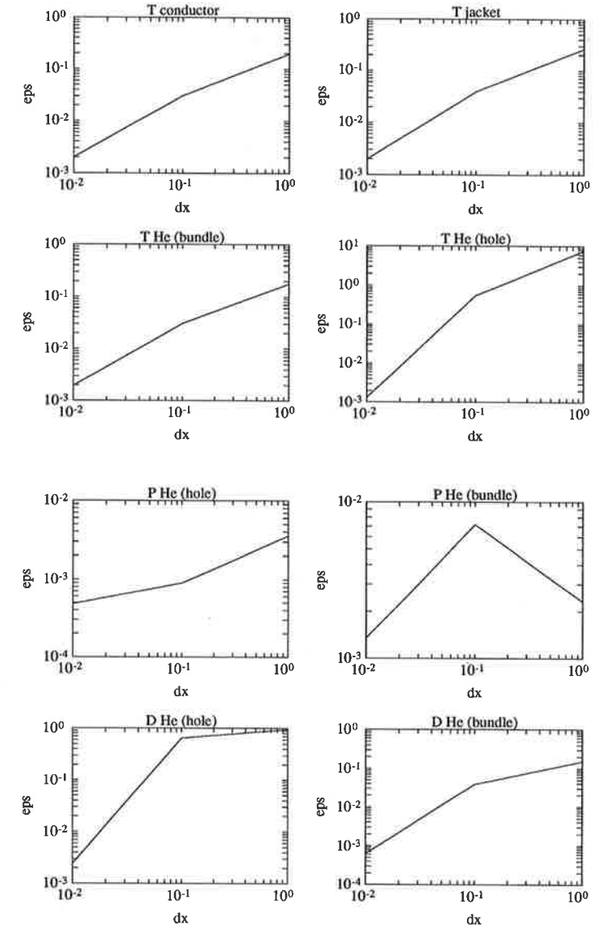

Fig. 6. Relative errors for several quantities at $x = 5$ m vs. Δx [m]. Case $\theta = \alpha_t = 1$, $\Delta t = 10^{-4}$s.

4. RESULTS OF COMPUTATIONAL TESTS

We have performed a set of tests of Mithrandir (some of the parameters used are shown in Table I). Both a typical behavior with and without mixing between the two fluids, and space/time convergence of the codes will be discussed. A CICC with $l = 10$m length was chosen, i.e., much shorter than typical; this was due to the fact that the reference ("exact") solution used for the convergence studies requires a fixed mesh with $\Delta x = 1$ mm, and a longer conductor would have needed too many elements from a CPU viewpoint; still, some im-

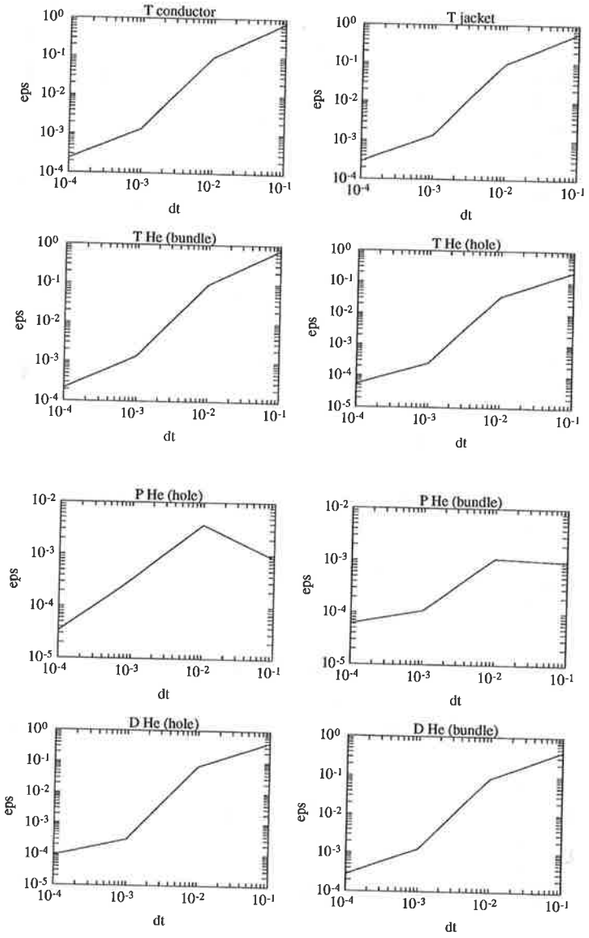

Fig. 7. Relative errors for several quantities at $x = 5$ m vs. Δt [s]. Case $\theta = \alpha_i = 1$, $\Delta x = 0.01$ m.

portant features as, e.g., normal front propagation speed (see Fig. 5), are similar to those encountered in a more realistic case. The strands were heated uniformly over a length of 0.2 m centred at $x = 5$ m, for a duration of 1s, with a resulting power $Q_{ext,Sl} = 2$kW. To this $Q_{Joule,Sl}$ is added, with an (x, t) dependence as given by the local strand resistivity to an imposed current of 8kA.

4.1. Short-Term Transient with Segregated Hole (Separate Fluids)

The first set of simulations, and all of the convergence results, refer to the case of a central cooling hole delimited by an impermeable wall. Since in this situation all mixing terms in Eqs. (1–3) vanish, one-fluid models would hardly be applicable here. A transient of 1s duration was considered and some of the resulting space and time profiles are shown in Figs. 1–5.

We notice that at the center of the heating region all temperatures increase (Fig. 1a) and vice-versa both He fluids expand (Fig. 1c) monotonically in time due to the heating, hole quantities varying very little due to the weak coupling of the He there with the rest of the CICC. The evolution of the central pressure of the bundle He (Fig. 1b), on the contrary, has the character of a damped oscillator. After O(1s)p^β ($x = 5$m) is steady and slightly

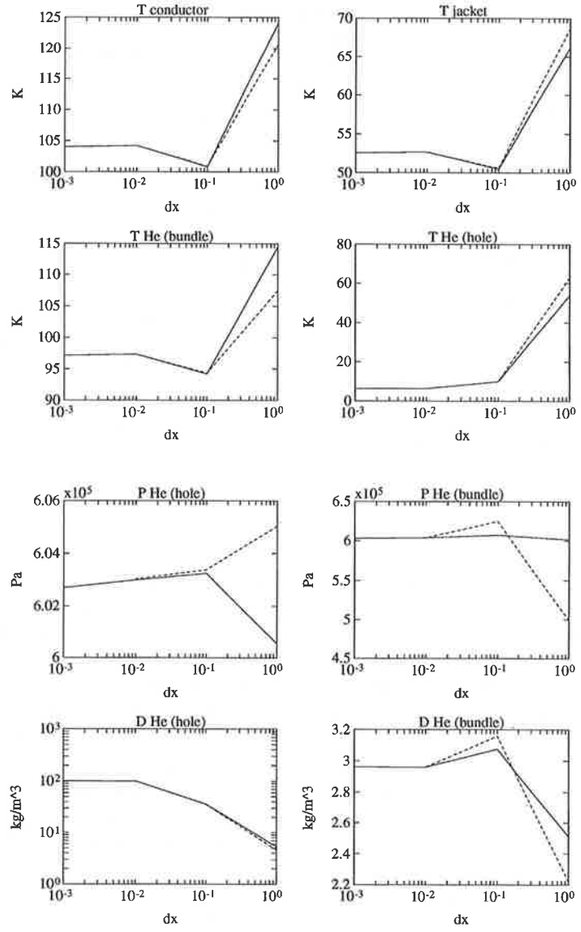

Fig. 8. Several quantities at $x = 5$ m vs. Δx [m]: $\Delta t = 10^{-4}$s (solid lines), adaptive Δt (dashed lines). Case $\theta = \alpha_i = 1$.

above the initial (and boundary) value. Numerical experiments performed parametrically changing the hydraulic diameter D in the range between 10^2 and 10^{-3} times the nominal value have shown that the oscillation is not of numerical nature but is related to the balance between friction and inertia: at $D \sim 0.1$ times the nominal value, i.e., with stronger friction, the oscillations disappear. A simplified analysis of this problem shows that the damping mechanism is nonlinear, and related to the compression $\partial v^\beta/\partial x$ at the center.

The initial evolution (first 0.025 seconds) of the $p^\beta(x)$ profiles (Fig. 2a) shows the pressure front(s) propagating at the sound speed towards the conductor end(s), a behavior previously observed in;[9] the profiles of other He quantities (not shown) evolve similarly on that time scale. On the ''longer'', 1s time scale pressures and flows (Figs. 2b-d) evolve coupled, with v^β and v^H reaching values O(1m/s) over most of the conduit.

Extremely steep temperature (Figs. 3a-d) and density (Figs. 4a,b) profiles develop in time, emphasizing the need for adaptive meshing. The ''Mole Antonelliana''[3] kind of shape results from the superposition of the imposed $Q_{ext,Sl}$, with the varying $Q_{Joule,Sl}$ which advances

[3] The 168m tall symbol of Torino, built 1863 from a design of A. Antonelli.

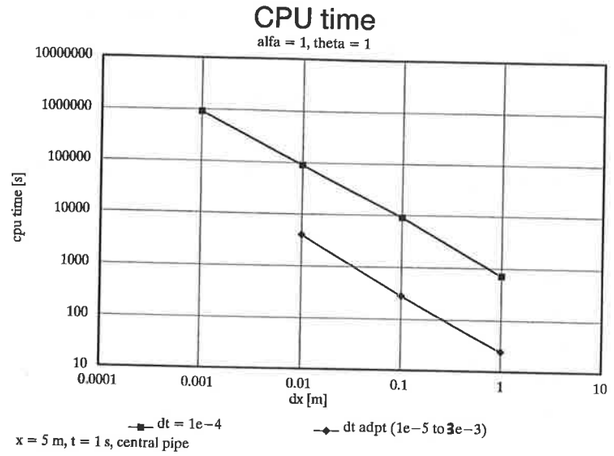

Fig. 9. CPU time per run [s] vs. Δx [m]: $\Delta t = 10^{-4}$s (upper line), adaptive Δt (lower line).

in x with the normal front. The dip in T^{gl} (Fig. 3a) has to do with the fact that at $x = 5$m the flow is stagnant due to symmetry, so that h_{eq} drops there to very low values, compromising the heat exchange between bundle and hole. We have also estimated that, notwithstanding the strong curvature of the profile there, heat conduction if included would contribute O(0.01%) to the heat balance, due to the extremely low (O(0.01W/m K))heat conductivity of He at that pressure and temperature.

All of the previous results have been obtained with $\theta = \alpha_i = 1$. The possibility of using a pure Galerkin ($\alpha_i = 0$) will be discussed in 4.1.3. From the point of view of the choice of θ we also tried $\theta = 0.5$, because in a scalar linear convection problem with numerical diffusion added as in Eqs. (8a,b) one can show that this would lead to quadratic convergence in time and inconditional stability; however, almost no damping is provided by such a scheme, particularly at very low (e.g., 0.01) or very high (e.g., 100) Courant numbers, whereas $\theta = 1$ damps the high frequencies, the larger the Courant number is. The results of our runs (not shown) were qualitatively consistent with this picture, and it typically was impossible to avoid unphysical space and time oscillations in the solution, unless a smaller Δt was used than in the $\theta = 1$ case.

4.1.1. Space Convergence

The space convergence of the code has been investigated by running it with different Δx values in the range 0.01/1m on a fixed (nonadaptive) mesh, using $\theta = \alpha_i = 1$ and fixed (nonadaptive) $\Delta t = 10^{-4}$ s. The relative error plots of Fig. 6 refer to computed values at $x = 5$ m and $t = 1$s compared with the values obtained using $\Delta x = 0.001$ m, which is used as reference (''exact'') solution. In Fig. 6, as well as in the following Figs. 7, 8, 10, a plot for each of the dependent variables of Eqs. (1–3,7) is shown, for the sake of completeness. It can be seen from the plots of Fig. 6 that the Galerkin scheme with O(Δx) numerical diffusion is more or less linearly convergent in space, as expected, obviously provided Δx is sufficiently small.

4.1.2. Time Convergence

The time convergence of the code has been investigated by running it with different (nonadaptive) Δt values in the range $10^{-1}/10^{-4}$ s, again using $\theta = \alpha_i = 1$, and fixed (nonadaptive) $\Delta x = 0.01$ m. The relative error plots of Fig. 7 again refer to computed values at $x = 5$ m and $t = 1$s compared with the values obtained using $\Delta t = 10^{-5}$s, which is used as reference (''exact'') solution. It can be seen from the plots that the fully implicit scheme is more or less linearly convergent in time, as expected, provided Δt is sufficiently small.

4.1.3. Effect of Adaptivity and Numerical Diffusion

We have investigated the effect of using an adaptive Δt. In Fig. 8 the convergence in space of the code

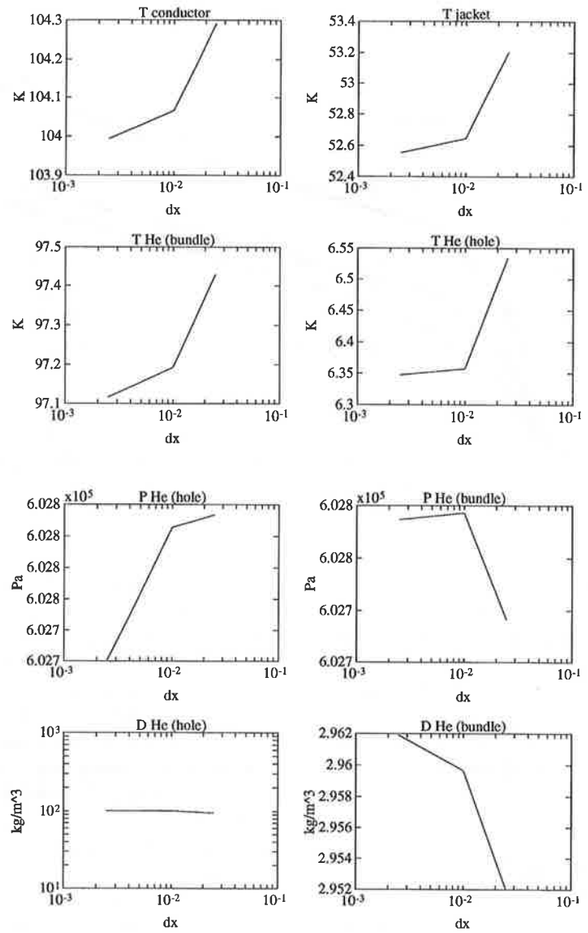

Fig. 10. Several quantities at $x = 5$ m vs. Δx [m]. Case $\alpha_i = 0$, $\theta = 1$, $\Delta t = 10^{-4}$s.

is demonstrated using both a fixed Δt (solid lines, same data of Fig. 6 although with a different representation) and an adaptive Δt (dashed lines). One sees that if Δx is sufficiently small the two choices lead to the same results; however (Fig. 9) the CPU time required for the same accuracy goes typically down by a factor of about 30, when using an adaptive Δt. (In these adaptive cases one starts with $\Delta t = 10^{-5}$s and reaches a maximum $\Delta t \approx 3 \times 10^{-3}$s). Notice also that, due to the use of a band matrix solver, the CPU cost increases only linearly with the number of elements.

We consider now the effect of using an adaptive Δx: it turns out that the accuracy one can obtain is more or less determined by the maximum Δx (of the fixed mesh). This is probably due to the fact that only the normal fronts are being followed by the mesh; large gradients near the pipe central section due to localized external heating, or related to other (non normal) propagating fronts, could not be resolved with the present adaptive algorithm, unless the background mesh is sufficiently fine. Further work on suitable error indicators will be devoted to this subject in the near future.

A limited amount of runs has been performed using the pure Galerkin scheme ($\alpha_i = 0$) with $\theta = 1$, and space convergence for this case is shown in Fig. 10. The major indications coming from the numerical experiments

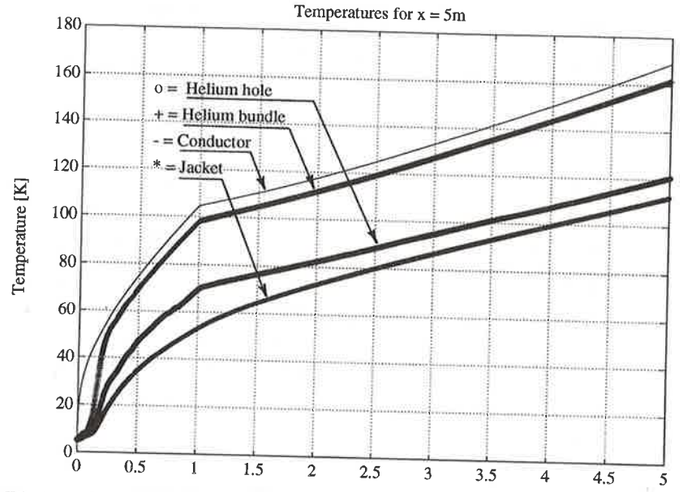

Fig. 11a. Temperatures [K] at $x = 5$ m vs. time [s]: strands (solid line), cable bundle He (+), jacket/conduit (*), hole He (○). Mixing fluids.

seem to confirm what would be expected[7] in similar but simpler cases (e.g., linear scalar convection): (1) the code converges more or less quadratically in space provided Δx is sufficiently small; (2) there is a (limited) range of Δx (e.g., 0.1 m) where pure Galerkin does not converge, whereas Galerkin plus numerical diffusion does, with errors of the order of a few % with respect to the best pure Galerkin solution (compare Fig. 10 with Fig. 8).

4.2. Long-Term Transient with Mixing Fluids

We have started a detailed study with Mithrandir of the important case when the He in the bundle and that in the hole can mix together through suitable perforations in the interface between cables and hole. A set of results for a long (5s) transient, representative of what has been obtained until now, is shown in Figs. 11–14. Here we assumed that the passage for the mixing extends uniformly to about 3% of the interface area, i.e., $A_\perp/(lD^H) \approx 0.03$, where D^H is the hydraulic diameter of the hole. Much larger fractions can lead to convergence difficulties which are currently under investigation. In order to better identify the effects of the mixing we also assumed $h_{eq} = 0$ for the present run.

The time evolution of the temperatures at $x = 5$m (Fig. 11a) can be compared for the first second with that in Fig. 1a: it is clear that the coupling between T^B and T^H is now fairly strong, so that T^H is being pulled up leading to differences O(30 K) after 1s, i.e., much smaller that in the case of a segregated hole. After 1s the external heating is turned off, which explains the change in slope of the curves.

The pressures at $x = 5$ m (Fig. 11b) are very tightly coupled, pressure equilibration occurring on the transverse sound time scale (O(1ms) in the present case). For the same input power as in the case of Sec. 4.1 we find now a lower peak, because part of the energy deposited in the bundle He can be relieved to the hole. The central pressure evolution again resembles that of a damped oscillator.

The time evolution of the T^H profile (Fig. 12a) shows a new feature compared to the case without perforations: a second front appears, faster than the normal one (see Fig. 14), whereas in T^B (Fig. 12b) only the normal one is present; this is due to the fact that (not shown) at, say, $t = 2s$, $v^B \sim 0.2 - 0.4\text{m/s} < v^{FRONT}$, whereas $v^H \sim 1.0 - 2.0\text{m/s} > v^{FRONT}$, for $x > 6$m. In the case of Sec. 4.1 no convective speed was larger than v^{FRONT} and the second front did not appear. It must also be noticed that (not shown) the He in the hole goes through the pseudo-critical line at this second front. This transition produces an overpressure responsible for the mixing backflow from hole to bundle (see Fig. 13), whereas the mixing flow from bundle to hole is localized near the normal front.

We finally remark that the normal front speed (see Fig. 14) is larger than v^B (probably because of heat conduction in the cables leading to a hybrid Peclet number

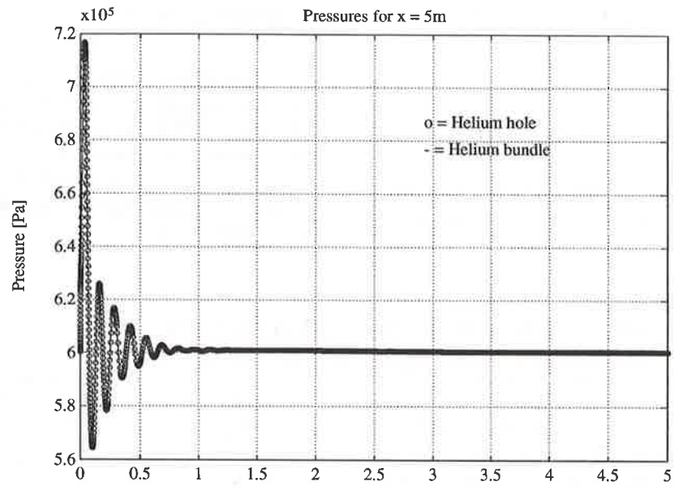

Fig. 11b. He pressures [Pa] vs. time [s]: cable bundle (solid line), hole (○). Mixing fluids.

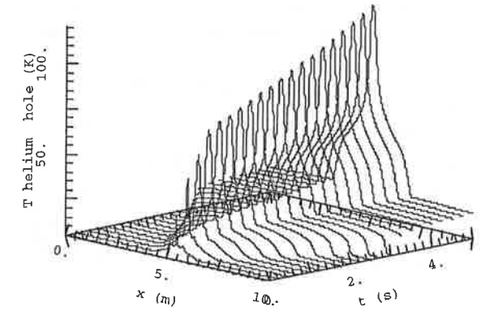

a

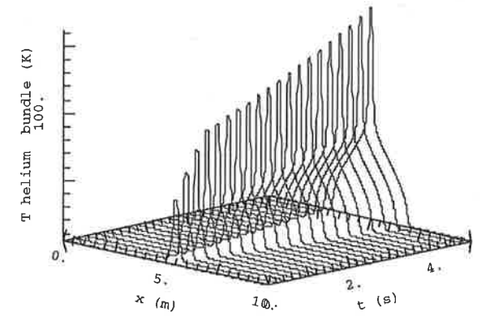

b

Fig. 12. Space/time temperature profiles: hole He (a), cable bundle He (b). Mixing fluids.

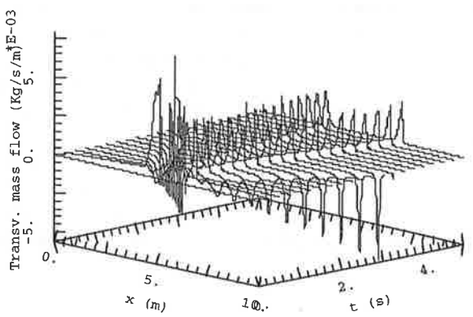

Fig. 13. Space/time profile of the transverse mass flow per unit length [kg/(m s)] (positive values from bundle to hole, negative vice-versa).

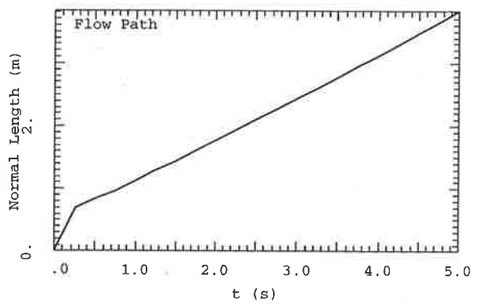

Fig. 14. Length of normal conducting region [m] vs. time. Mixing fluids.

O(1)), but is smaller than in the case without mixing (Fig. 5).

5. CONCLUSION AND PERSPECTIVE

A new two-fluid code, Mithrandir, has been developed for the simulation of thermohydraulic transients in superconducting magnets; the code has been applied to a CICC with central cooling hole and cross section parameters similar to that proposed for ITER.

A study based on numerical experiments has been performed for the case without mixing between the two fluids, and for a reduced conductor length $l = 10$m. It shows that the code converges both in space and time as expected from the analysis of simpler model problems. From the numerical point of view, Petrov-Galerkin stabilization, mesh adaptation and linearization of the equations are currently being investigated to further increase the robustness of the code.

A first comparison of the results obtained with and without mixing has been presented. The mixing model is presently rather rudimentary, so that the corresponding behavior predicted by the code is to be taken as indicative only. In the case presented here the code converges to reasonable time and space profiles, and interesting new features appear in the solution with mixing, compared to the case of two separate fluids.

Compatibly with the computer resources available we aim to the full scale testing of the mixing model on realistic conductor lengths; this should enable a meaningful simulation/validation of the QUELL experiments to be performed in the near future.

ACKNOWLEDGMENTS

Most of the computations have been performed on an IBM RS/6000 workstation of the NET Team (IPP Garching), and we gratefully acknowledge the support of E. Salpietro for making this computer time available to us. One of the authors (S.D.P.) thanks ASP Torino for partial financial support, and the NET Team for its kind hospitality during a stay at IPP Garching.

REFERENCES

1. L. Bottura, *A Quench Simulation Model for the ITER Magnets*, NET Report N/R/0821/54/A (1994); L. Bottura, *Thermohydraulics of CICC's with Central Cooling Passage*, IEEE Trans. Appl. Sup. **5** (1995) 745–748.
2. S. De Palo, L. Bottura and R. Zanino, *Computer Analysis of the Thermo-hydraulic Measurements on CEA Dummy Cables Performed at CEN-Grenoble*, this issue.
3. C. A. Luongo, C. L. Chang and K. D. Partain, *A Computational Quench Model Applicable to the SMES/CICC*, IEEE Trans. Mag. **30** (1994) 2596–2572.
4. V. Arp, *Thermodynamics of Single-Phase One-Dimensional Fluid Flow*, Cryogenics (1975) 285–289.
5. B. A. Hands, *HEPROP—A Computer Package for the Thermophysical Properties of Helium down to about 2K* Cryogenics **13** (1973) 423–425.
6. A. E. Long, *Transverse Heat Transfer in a CICC with Central Cooling Channel*, Master's Thesis, Dept. of Mech. Engineering, MIT (1995) (unpublished).
7. O. C. Zienkiewicz and R. L. Taylor, *The Finite Element Method*, Vol. 2 (McGraw-Hill, London, 1991).
8. A. Shajii and J. P. Freidberg, *Quench in Superconducting Magnets. I. Model and Numerical Implementation*, J. Appl. Phys. **76** (1994) 3149–3158.
9. V. Arp, *Stability and Thermal Quenches in Force-Cooled Superconducting Cables*, Proc. of 1980 Superconducting MHD Magnet Design Conf., MIT, 142 (1980).

Journal of Fusion Energy, Vol. 14, No. 1, 1995

Investigation on Effects of Conductor Concepts on 3D Quench Propagation in Superconducting Coils Using the Code System MAGS[1]

R. Meyder[2]

Quench propagation is analysed for two different conductor types, foreseen for a Tokamak and a Stellarator type fusion machine, respectively. For the analysis the code system MAGS is used. In the paper MAGS is presented briefly. The analysis considers quench in a small layer wound coil with separate coolant flow in the two layers modelled. Quench is initiated in the first layer and propagates in this coolant channel as well as to the second coolant channel, via heat conduction. Due to the different design, very different front velocities and peak pressures were determined.

KEY WORDS: Superconducting coils; quench analysis; forced flow cooled.

1. INTRODUCTION

The determination of the propagation velocity of normal conducting zones in a superconducting coil (quench) is important as well for the design as for safety considerations. While for aspects of stable operation the margin to quench should be large, a normal conducting zone in a too stable conductor may be not detected in time in order to take mitigating actions, especially with a local quench. This question has led to the development of models to calculate the quench behaviour of superconductors, especially for forced flow Helium cooled cable in conduit conductors.

The different aspects mentioned have also lead to different tools for this analysis. Some codes, like SARUMAN[5] or GANDALF[2] are codes prepared for design analyses, while others, e.g., MAGS,[7] being presented in this paper, has been developed to model complex coil accidents including quench. To give some idea on the tools available in MAGS, Table I gives a short overview of the present status.

In this paper two different coil designs, i.e., an ITER CS typical and a Wendelstein 7-X typical design, are analysed in their quench propagation behaviour. It is to be stated that each coil design has reasons why it looks as it is, others than its quench propagation behaviour. Therefore this analysis does not intend to make a ranking of the two designs, it is rather a simple comparison of their behaviour.

The characteristic data of the two designs are given in the Table II.

For the analysis the data for the Wendelstein conductor are slightly changed, the magnet field is set to 5 T, the coolant temperature is set to 4.0 K and the mass flux is 0.8 g/s.

A small coil is considered consisting of 16 turns in two layers. The coolant flow is separate for each layer. Total length of the coil is 100 m. In the centre of layer 1, i.e., in the last circumferential mesh element of turn 4 (Q.I.1) and in the first circumferential mesh element of turn 5 (Q.I.2), a propagating quench is initiated. Current and magnet field are constant with time and space.

[1] Presented at the Workshop on Computation of Thermo-Hydraulic Transients in Superconductors, Lausanne, June 6–8, 1995.

[2] Institut für Reaktorsicherheit, Forschungszentrum Karlsruhe, Technik und Umwelt, Postfach 3640, D-76021 Karlsruhe.

0164-0313/95/0300-0041$07.50/0